Aberystwyth University

Exciplex emission from electroluminescent ladder-type pentaphenylene oligomers bearing both electron- and hole-accepting substituents

Finlayson, Christopher Edward; Kim, Ji-Seon; Liddell, Matthew J.; Friend, Richard H.; Jung, Sung-Hyun; Grimsdale, Andrew C.; Muellen, Klaus

Exciplex emission from electroluminescent ladder-type pentaphenylene oligomers bearing both electron- and hole-accepting substituents

Chris E. Finlayson, Ji-Seon Kim, Matthew J. Liddell, Richard H. Friend, Sung-Hyun Jung, Andrew C. Grimsdale, and Klaus Müllen

Exciplex emission from electroluminescent ladder-type pentaphenylene oligomers bearing both electron- and hole-accepting substituents

Chris E. Finlayson,[a] Ji-Seon Kim, Matthew J. Liddell, and Richard H. Friend[b]
Cavendish Laboratory, JJ Thomson Avenue, Cambridge CB3 0HE, United Kingdom

Sung-Hyun Jung, Andrew C. Grimsdale,[c] and Klaus Müllen[d]
Max-Planck-Institute for Polymer Research, Ackermannweg 10, 55128 Mainz, Germany

We examine the photophysical properties of ladder-type pentaphenylenes, which have been prepared as prototypical "all-in-one" emissive materials bearing both electron-accepting (diaryloxadiazole) and electron-donating (triphenylamine) units. We find that donor-acceptor interactions are very dependent on the nature of the connectivity of these groups to the main pentaphenylene chain. When the oxadiazole and triphenylamine units were substituted on opposite sides of the π-conjugated pentaphenylene chromophore, photoluminescence with long lifetimes typical of exciplex-like species was observed, while being significantly quenched by intermolecular charge separation between the substituents. By contrast, when the triphenylamine units were attached at the ends of the chromophore, no such effects were observed and a blue/green photoluminescence was obtained with very high quantum efficiency. In this latter configuration, evidence of ambipolar charge transport and a blue/green electroluminescence were additionally observed. © *2008 American Institute of Physics*. [DOI: 10.1063/1.2813351]

I. INTRODUCTION

Further to our recent studies of poly(ladder-type pentaphenylene)s[1,2] as photostable materials which emitted pure blue light [Fig. 1(a)], it was considered that ladder-type pentaphenylene oligomers, bearing both oxadiazole and triphenylamine substituents, would represent an interesting category of prototypical molecular materials containing an emissive chromophore and both hole- and electron-accepting moieties. Such "all-in-one" materials might serve both as analog structures for more complex supramolecules, model compounds for new polymers, or as emissive materials in their own right. Of particular interest are the mechanisms of charge/energy transfer and of radiative recombination in such simplified systems, both at the intra- and intermolecular levels. In order to investigate the effect of the relative positions of the charge transporting groups upon the optical, photophysical, and electronic properties, we aimed to prepare both a molecule with the oxadiazole acceptors on the bridgeheads and the triphenylamine donor units at the ends of the molecule (structure "A" or compound 10 in Appendix) and one with the two charge-accepting units on directly opposite sides of the chromophore (structure "B" or compound 7 in Appendix). This approach of positioning the moieties on the bridgeheads contrasts with previously reported structures, where these functional groups are directly linked by conjugation to the main chromophoric unit[3] or positioned in dipolar pendant groups.[4] In this paper, we report upon our pho-

tophysical studies of these systems and demonstrate that the two materials under scrutiny show surprisingly different behavior, in terms of optical and photophysical properties. Our experiments demonstrate that the donor-acceptor interactions are very dependent on the nature of the connectivity of these groups to the main pentaphenylene chain and, in particular, we observe emission from exciplexlike states of these molecules. While the phenomena of exciplex formation at heterojunctions have been very well documented for systems of conjugated-polymer blends,[5,6] the reported observation of such effects in small chromophoric molecules is comparatively rare.

We note that it has previously been shown that attachment of hole-accepting triphenylamine groups as substituents on the bridgeheads[7] or as chain-terminating groups[8] in polyfluorenes (PFs) improves their efficiency in light-emitting diodes (LEDs). The electron-accepting properties of PFs have similarly been enhanced by incorporating fluorenes with aryloxadiazole moieties at the bridgehead positions,[9] and copolymers containing both units bearing oxadiazoles and units with triphenylamine substituents have also displayed particularly high electroluminescence efficiencies.[10] The electroluminescent properties of these prototypical all-in-one materials were also investigated using simple LED configurations. Additionally, a reference material [structure "C," as shown in Fig. 8(b)], consisting of a bridged pentaphenylene with simple phenylene termination of the bridgeheads, was also studied by way of comparison. The observation of an intense blue or blue/green electroluminescence (EL) in these structures suggests that these materials represent a new and interesting category of oligomeric semiconductors for future application in LEDs. Complementary studies in thin-film transistor (TFT) configurations provided

[a] Electronic mail: cef26@cam.ac.uk.
[b] Electronic mail: rhf10@cam.ac.uk.
[c] Present address: School of Materials Science and Engineering, Nanyang Technological University, Nanyang Avenue, Singapore 639798.
[d] Electronic mail: muellen@mpip-mainz.mpg.de.
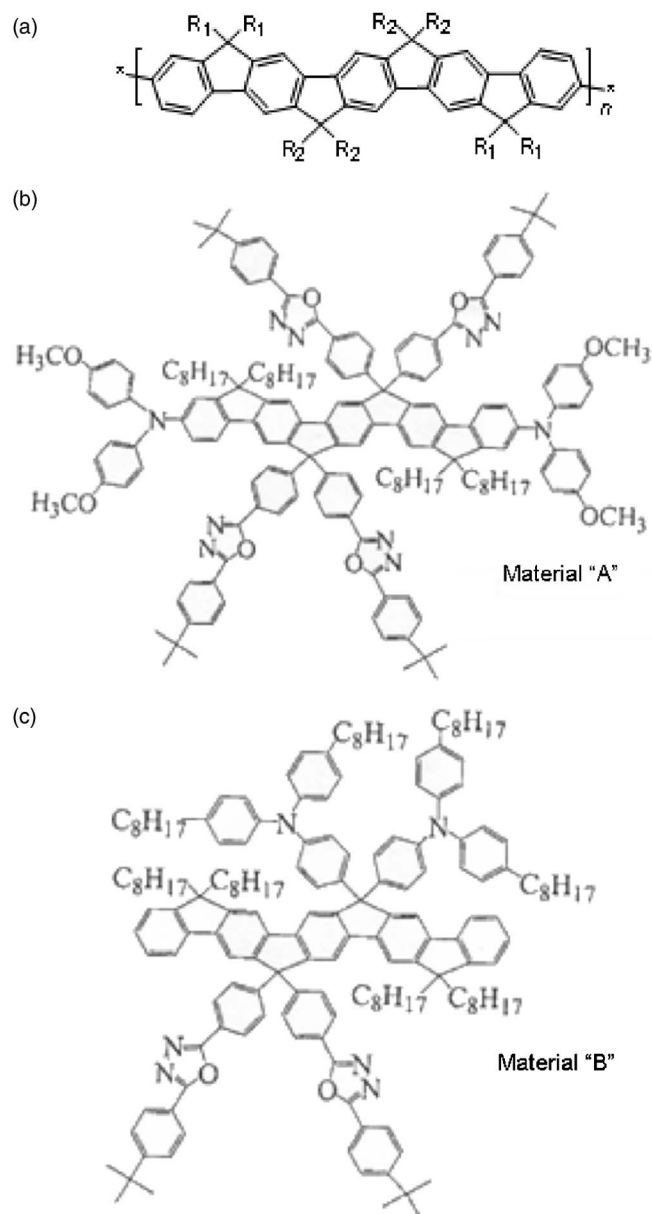
(a)

(b)

Material "A"

(c)

Material "B"

FIG. 1. (a) the chemical structure of a typical blue-emissive bridged polyphenylene, where the bridgeheads are substituted with aryl and/or alkyl groups. The structures of the two substituted pentaphenylene oligomers described in this paper are shown in (b) material "A" and (c) material "B." The reference material (material "C"), which was also studied for comparison, consisted of a bridged pentaphenylene with simple phenylene termination of the bridgeheads.

further insight into the electronic transport properties of these materials, and cyclic voltammetry analysis showed the electrochemical characteristics of these materials to be within a suitable range for both electron- and hole-injection processes.

II. EXPERIMENTAL

The detailed methodology of synthesis for the pentaphenylene structures described in this paper is given in Appendix. Scheme 1 illustrates the synthetic route for the preparation of the tetraadduct and diadduct pentaphenylene. 2-(4-bromophenyl)-5-(4-*tert*-butylphenyl)-1,3,4-oxadiazole was prepared by dehydrative cyclization of the 1-(4-

bromobenzoyl)-2-(4-tert-butylbenzoyl) hydrazine using $POCl_3$. The pentaphenylenediester 1 was synthesized according to the literature procedures by using Suzuki coupling of the fluorene-2-boronate ester with the dibromoterephathalate.[1] The key step in the synthesis of two ladder-type pentaphenylenes was the addition of excess diaryloxadiazole monolithium 2 to the diester 1 as shown in Scheme 1. Interestingly, this gave a mixture of the tetraadduct 3 (42%) and the diadduct 4 (33%), which were separable by column chromatography. Ring closure of the diadduct 4 using boron-trifluoride etherate gave the pentaphenylene 5 in 78% yield. 4-bromo-N,N-bis(4-n-octylphenyl)aniline was synthesized by N-bromosuccinimide-bromination of the 4,4'-dioctyl-triphenylamine, which was synthesized from aniline and two equivalents of 1-bromo-4-octylbenzene in one pot using the palladium-catalyzed amination reaction as described previously. Addition of a lithiated dialkyltriphneylamine 6 followed by ring closure with boron-trifluoride etherate then produced the pentaphenylene 7 (21%, two steps) with oxadiazole and triphenylamine substituents directly opposite each other (Scheme 2). Ring closure of the tetraadduct 3 to form 8 proceeded in 89% yield (Scheme 3). Bromination with bromine afforded the dibromide 9 (76%) which underwent Buchwald-Hartwig amination with di(4-methoxyphenyl)amine to give the amine-end-capped pentaphenylene 10 in 62% yield.

The final structures, A (compound 10) and B (compound 7), were shown in Fig. 1, and were subsequently confirmed by ^{1}H NMR analysis; in particular, the well defined nature of the peaks associated with aryl-H groups on the backbone indicated that these materials had been prepared in an undoped form, as intended.

III. PHOTOPHYSICS

We obtained the absorption and photoluminescence (PL) spectra of materials A and B in solvents of varying polarity to investigate the intramolecular properties of these donor-acceptor molecules; in particular, how the side group moieties interact with the conjugated backbone (and each other) in the two cases. The UV-visible absorption spectra of A and B are shown in Figs. 2(a)–2(c) and show markedly different optical behavior. The end-capped compound (material A) was measured in acetone and dichloromethane only, due to insolubility in cyclohexane, displaying an absorption peak at $\lambda=436$ nm in acetone and $\lambda=441$ nm in dichloromethane with a sharp absorption edge typical of a ladder-type oligophenylene.[11] The position of the peak is strongly red-shifted compared with non-end-capped pentaphenylenes due to the arylamine end groups being conjugated into the ends of the pentaphenylene backbone via an sp^2 hybridization of nitrogen orbitals, which acts to increase the overall backbone-conjugation length. By contrast, B gave three distinct absorption peaks (λ_{max}): one near 350 nm, another in a range of 465–477 nm, and the other in a range of 677–720 nm. The former peak is assigned to a π-π^* transition mainly occurring in the pentaphenylene backbone, whereas the relatively large oscillator strength
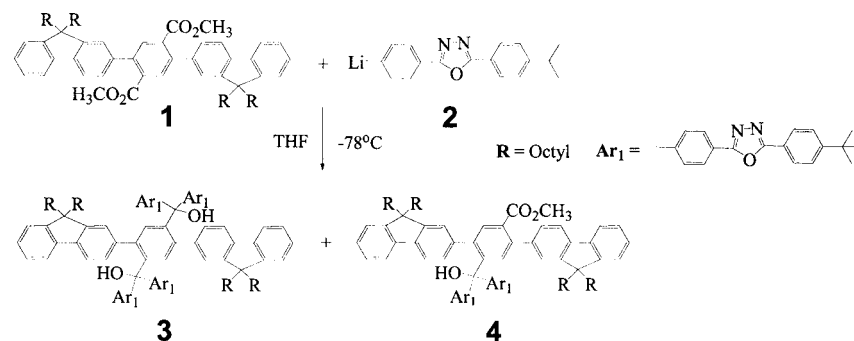
SCHEME 1. Synthetic route for the preparation of the tetraadduct and diadduct pentaphenylenes.

($\varepsilon > 10^4$ 1/mol cm) of the lower-energy peaks are reminiscent of effects due to intramolecular charge-transfer absorption[12–14] or charge-separated state (e.g., polaron) absorption.

The PL spectrum of B in various solvents (acetone, dichloromethane, and cyclohexane) is exhibited in Fig. 2(c). Whereas A produces blue/green PL with an emission maximum around 500 nm in both acetone and dichloromethane, the emission from B is strongly solvent dependent. The PL spectra in the case of B show several different features, somewhat in contrast to what would be expected for a purely electronic transition. In the nonpolar cyclohexane, the spectrum is dominated by a series of peaks around $\lambda = 400-450$ nm, but in more polar solvents the spectrum is broader and redshifted, with significant green emission. Using a technique of quantitative fluorimetry,[15] with an ethanolic solution of the dye Rhodamine 6G as reference, the PL quantum efficiencies of B in chloroform and acetone were determined to be 4% and 2.6%, respectively. In contrast, a very high efficiency of 91% was found for A in chloroform. This apparent strong quenching of luminescence in the case of B is further evidence of collective donor-acceptor moiety interactions.

In Fig. 3(a), the concentration dependence of the photoluminescence from B in acetone is investigated. This clearly shows the emission as consisting of two discrete bands, a narrow feature at 400–420 nm and a broader tail from 450–650 nm (the "long wavelength tail" described previously), with the relative intensity contribution from each being clearly dependent on concentration. The two main short-wavelength features at 403 and 424 nm are, with varying relative intensities, present in each of the solvent media. The

shorter wavelength component predominates at higher concentrations, indicating this to be emission from a collective species (aggregates or similar). We note that the spectral shifts of the emission with varying concentration are generic within the range of solvents used; however, the equilibrium constant between components is different in each case. The data taken with acetone as the solvent give the best experimental demonstration of these effects within the dynamic range of the fluorimeter being used. These steady-state measurements give some indication of whether the process of intermolecular binding leads to the formation of a system with two discrete phases or whether a dynamic equilibrium exists between monomers and aggregates in solution. In particular, the apparent concentration dependence of the relative contributions to the optical properties of inter- and intramolecular components is indicative of a dynamic equilibrium. If we were dealing with a two-phase system, there is no reason why the fractional concentration of monomers should increase on account of dilution, in the absence of any strong solvent interaction. As a further direct demonstration of the equilibrium which exists in solution, thin-layer chromatography (TLC) was carried out on the materials A and B, using 50 μm silica-gel plates and acetone as the eluent under standard methods and conditions. Material A straight forwardly gives a single component, with a measured retardation factor (Rf) of 0.88, which is clearly photoluminescent under UV-A illumination. Similarly, material B is seen to give a well-defined photoluminescent component with an Rf of 0.86, but also a continuum of nonemissive "dark" components with Rf values ranging between 0.69 and 0.84. If the emissive and dark components on the plate are carefully divided by cleaving the plate, the components can be redissolved to allow
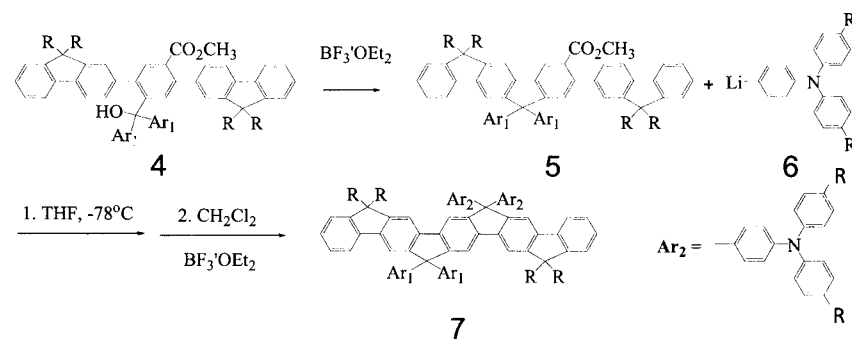
SCHEME 2. Preparation of structure B (compound 7) from diadduct pentaphenylene.
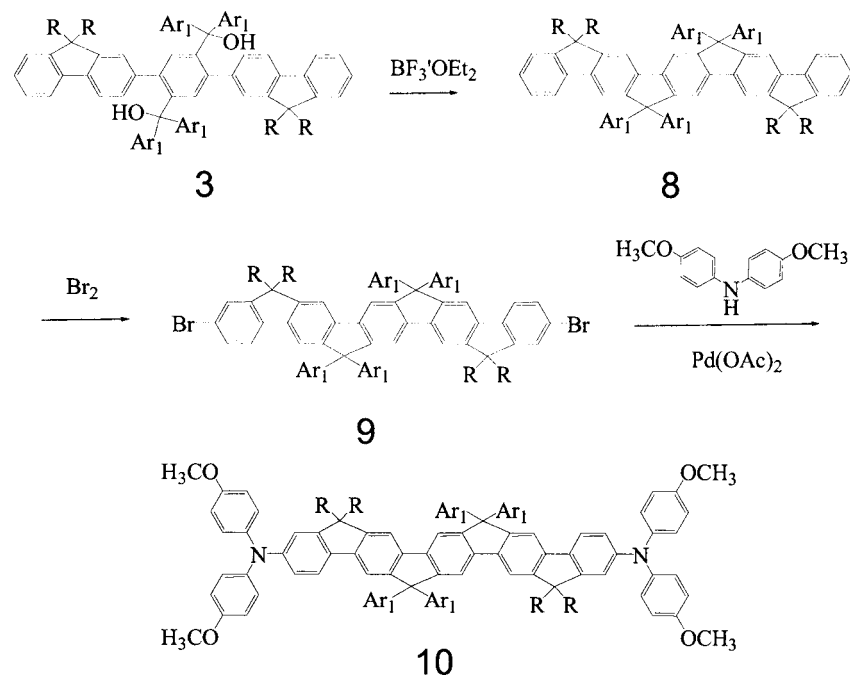
SCHEME 3. Preparation of structure A (compound 10) from tetraadduct pentaphenylene.

further separate TLC analysis. It is found that the chromatograms produced from the two components both also gave emissive bands at Rf=0.85 and a continuum of darker components with smaller retardation factors. It is likely that the diffuse nature of the dark zones on these TLC plates is indicative of the ill-defined molecular weight and adsorption affinity of aggregates or packed arrangements in solution. Additionally, the absorption spectra of the two redissolved components from the primary TLC experiment are found to be very similar to each other and to the original spotting solution of compound B.

In order to investigate the effects of change in chemical environment on the optical properties of compound B, and, in particular, the effect of a reducing or "oxygen-scavenging" environment, thin films of the material were spin coated onto quartz substrates and the absorption spectrum was measured before and after exposure to hydrazine vapor (partial pressure of 14 mm Hg, within an evacuated Schlenk line, for 1 h). As shown in Fig. 3(b), this exposure to hydrazine causes the long wavelength absorption band to disappear and a commensurate color change from dark green to colorless is observed. We therefore believe that the ability of material B to form this dark aggregated component is mediated by a chemical change, such as an oxidative process, as such a molecule is not expected to exhibit an energetically stable ground state, where charge is transferred between moieties; this is further corroborated by the quantum-chemical calculations described later in this paper. It is anticipated that further work, using transient absorption spectroscopy, may help to elucidate the detailed dynamics of the charge-transfer interactions between monomers.

Figure 4 shows time-correlated single photon counting (TCSPC) measurements[16] were carried out on dilute solutions of both compounds A and B and at an excitation wavelength of 407 nm. Luminescence lifetimes, at a series of dif-

ferent wavelengths, were derived from least-squares fitting of exponential decay functions to the data. In the case of A, we observe a decay lifetime of 1.43 ($\pm$0.04) ns, which is independent of the emission wavelength and, as might be expected for excimerlike emission from a π-conjugated system, no clear signs of any bi- or polyexponential behavior. In the case of B, however, we see differences in the behavior of the two (previously described) PL emission bands and a shift of the overall emission to longer wavelengths with time, as is possibly indicative of the presence of competing decay channels, and a relaxation into exciplexlike emissive states. The shorter wavelength component (centered at ~450 nm), which we have previously attributed to aggregated species, shows a clear biexponential decay with characteristic lifetimes of 1.35 and 9.18 ns, the longer of which is strongly suggestive of emission from an exciplexlike state,[17,18] and the longer wavelength (~505 nm) tail has a monoexponential lifetime of 3.94 ns. Taken in context with the concentration dependence of the PL emission spectra, this is clear evidence of exciplexlike species, formed between intermolecular aggregates.

Cyclic voltammetry (CV) studies[19] were carried out in order to investigate the relative reduction and oxidation potentials of the various substituents associated with compounds A and B, and this data is shown in Fig. 5(a). The materials were drop cast into films on a platinum electrode and the experimental configuration involved a perchlorate/Pt counter electrode, an internal ferrocene/ferrocenium standard, and a data scan rate of 100 mV/s. In reduction, the two compounds show very similar behavior, with a broad peak on the left-hand side of the CV plot corresponding to the reduction potential of the oxadiazole electron acceptor groups. In oxidation, both plots reveal a sharp peak corresponding to oxidation of the ground-state highest occupied molecular orbital (HOMO) level. In the case of A, the event
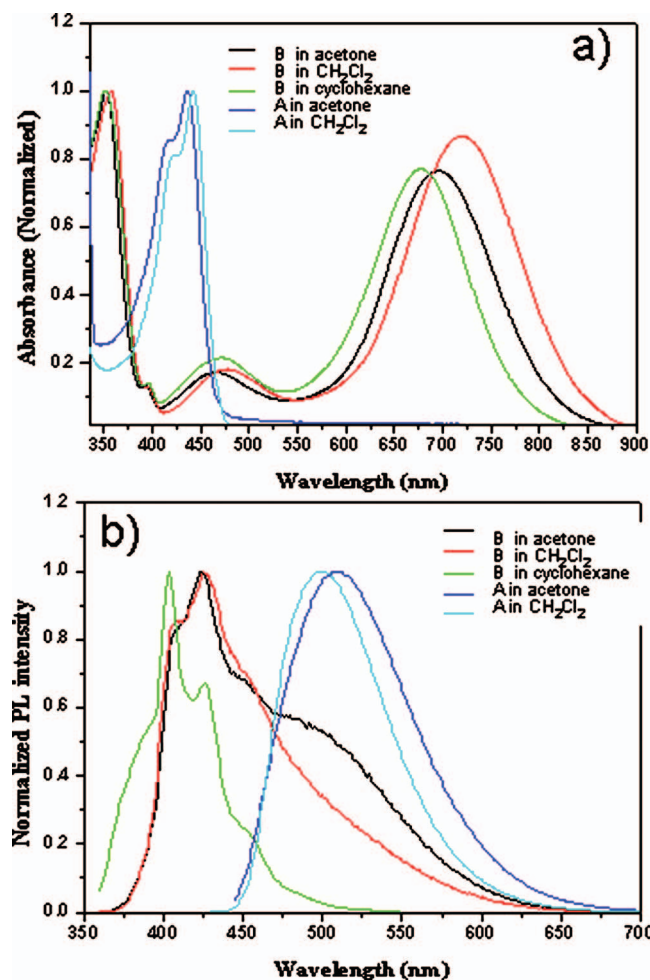
FIG. 2. (Color) (a) Absorption spectra for pentaphenylene compounds A and B in a range of solvents of varying polarity. In (b), the corresponding photoluminescence (PL) spectra for A and B are shown.

FIG. 3. (Color online) (a) shows how the photoluminescence spectrum of B varies with concentration in the approximate range from 1 to 100 μM in acetone. (b) Absorption spectra of a thin solid film of material B, both before and after treatment with hydrazine vapor (N_2H_4).

onset was observed to occur at around +0.4 V, relative to the standard, indicating a HOMO level energy of ~5.2 eV. For material B, the onset was at +1.1 V, giving a HOMO energy of ~5.9 eV. The shifting in position of these peaks relative to each other corresponds very closely to the redshifting of the π-π^* transition of A with respect to B, as shown in Fig. 2, and is a further consequence of the change in conjugation length due to the positioning of the electron-donating groups at the ends of the back-bone. A further oxidation two peaks are observed in the CV plot for B, which are close in energy to the HOMO event; these are weak or absent in the case of A and are attributable to the chemical oxidation effects previously described. Of particular interest, in terms of the facility with which holes may be injected into the material in operational LED devices, is the relative electrochemical positioning of the HOMO levels. The low-lying HOMO levels of many blue-emitting conjugated polymers, relative to standard electrode materials such as indium-tin oxide (ITO), have been long viewed as a significant fundamental limitation to device function.[20,21] In the case of material A, with a HOMO level of −5.2 eV, the barrier to hole injection from ITO is expected to be particularly favorable.
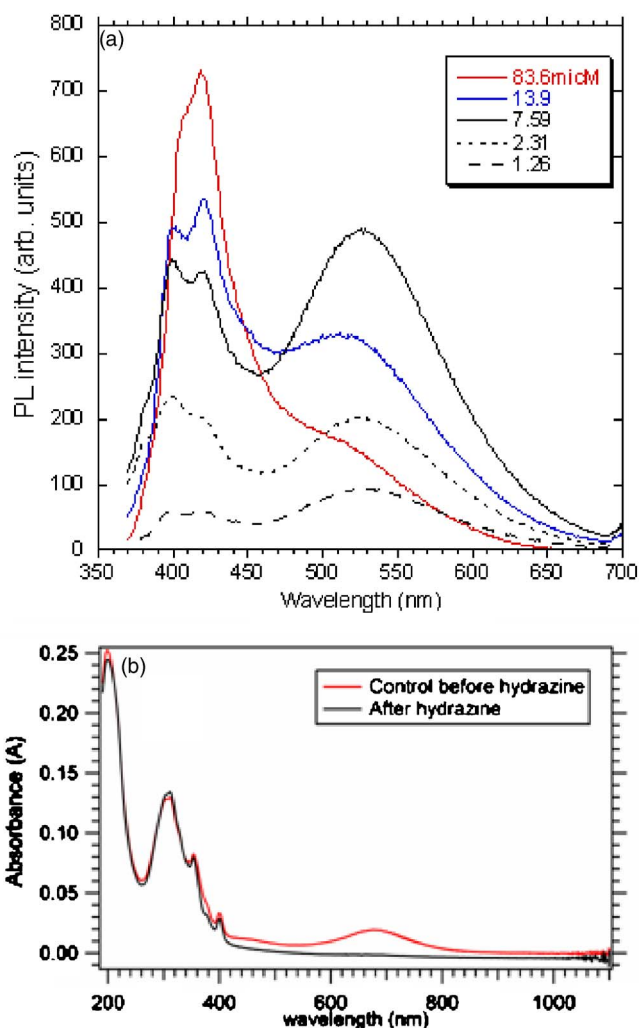
IV. COMPUTATIONAL ANALYSIS

Quantum-chemical calculations have been performed based on semiempirical approaches to understand the electronic structure and associated optical properties of the materials studied here. The ground-state geometry of the molecules was first optimized at the semiempirical Hartree-Fock Austin Model 1 (AM 1) level[22] in the gas phase (in the calculations, the alkyl side chains attached to the conjugated backbone were replaced by hydrogen atoms). In Fig. 6, these optimized three-dimensional structures are shown, and may be compared with the corresponding two-dimensional representations from Fig. 1. Of note in the 3D structures is the arrangement of the arylamine and oxadiazole side groups around the spirocarbon bonds attached to the backbone. In the case of A, a tetrahedral-like bonding arrangement around the spirogroups is predicted with pairs of oxadiazole electron-donating units projecting above and below the plane of the conjugated backbone. There is also some out-of-plane torsion of the end phenyl groups in the electron-donating units on the backbone ends. The tetrahedral arrangement of side groups around the spirocarbons in the case of B is simi-
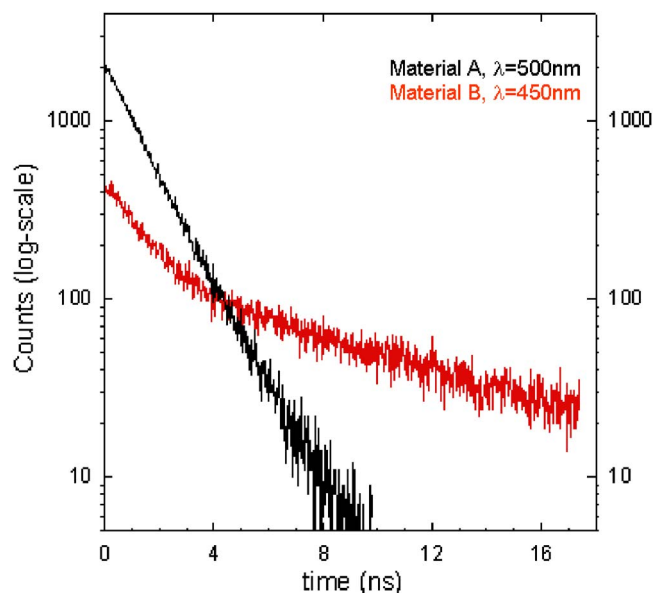
FIG. 4. (Color online) Time-correlated single photon counting (TCSPC) data, for dilute solutions of compounds A and B in acetone, as detected at PL emission wavelengths of 500 and 450 nm, respectively. Least-squares fitting of exponential decay functions to the data, giving a monoexponential decay with lifetime 1.43 ($\pm$/-0.04) ns in the case of material A and a biexponential decay with lifetime components 1.35 ns (27.8%) and 9.18 ns (72.2%) in the case of material B.

lar; with pairs of electron-donating and electron-accepting units, displaced by one phenyl ring along the backbone, projecting above and below the backbone plane.

Based on these optimized geometries, the electronic structure of the molecules was calculated by using the spectroscopic version of the semiempirical Hartree-Fock intermediate neglect of differential overlap (INDO) method.[23,24] Our modeling indicates that, although HOMO levels are localized in different ways for structures A and B, as shown in Figure 6, there is no evidence of conjugation linkage through the

FIG. 6. (Color) (top) AM1-optimized three-dimensional geometries for these molecules are displayed for structures A and B, showing the position and orientation of the side groups relative to each other and the conjugated backbone (O=red, N=blue, and C=gray). (middle) Energy and shape of the HOMO orbital for A and B calculated at the INDO level; the size and color of the circles describe the amplitude and sign of the linear combination of atomic orbitals coefficients associated with the atomic π orbitals. (bottom) Net charge density of S1 state for A and B, showing the symmetrical distribution of net positive (red) and negative (blue) charges.
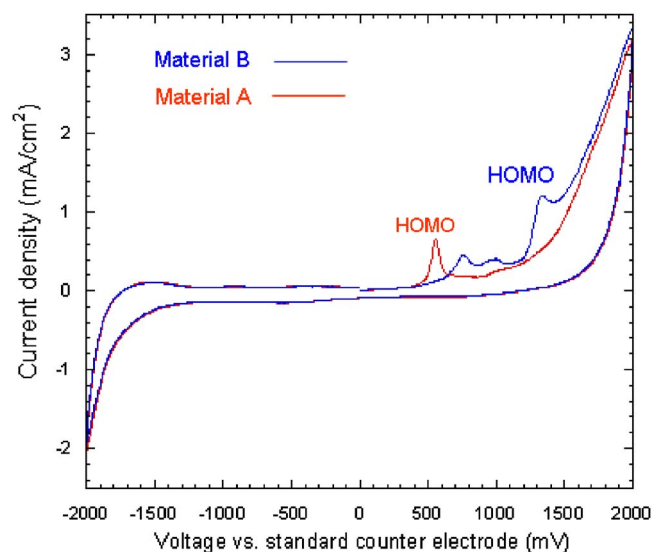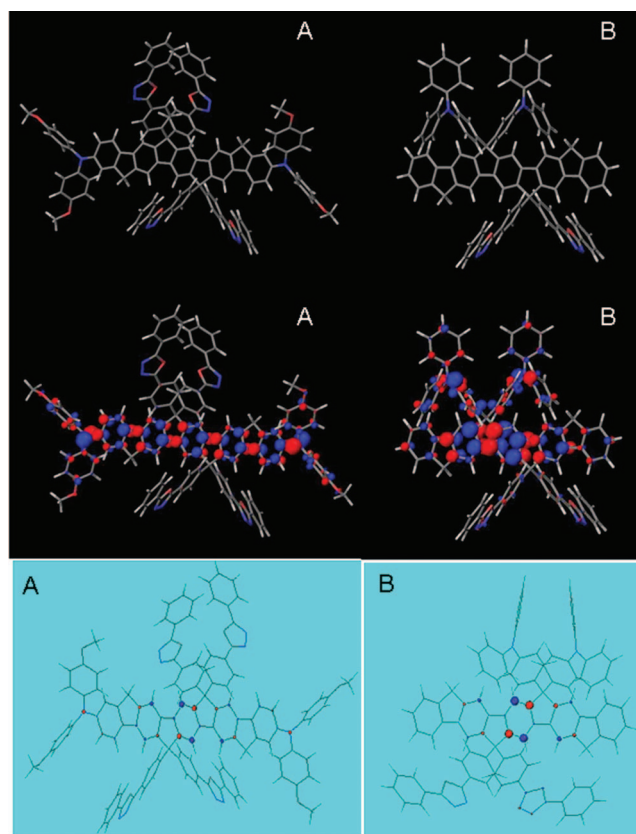

FIG. 5. (Color online) Cyclic voltammetry data for drop-cast films of materials A and B on platinum, with a scan rate of 100 mV/s. The counter electrode was perchlorate/Pt and an internal ferrocene/ferrocenium standard was used. The relative positions of the inferred HOMO levels for the two pentaphenylene materials are indicated for clarity.

spirocarbon bonds into the side group moieties in either structure. As may be seen from net charge densities of the first optical transitions (S1), net positive and negative charges are arranged symmetrically along the molecule in both cases; hence, there are no significant signs of charge separation in these ground-state optimized geometries.[25,26] The absorption spectra of all the molecules were also simulated by combining the INDO method to a single configuration interaction (SCI) scheme.[27] Figure 7 shows predictions of the relative oscillator strengths of highest occupied molecular orbital–lowest unoccupied molecular orbital transitions for both A and B, based on the calculated electron and hole wave functions of initial and final states. These are seen to be in reasonable agreement with the experimentally measured absorption spectra in Fig. 2 and provide confirmation of the redshift in the first absorption peak for structure A, due to the longer π conjugation along the backbone.

These models hence reaffirm that the observed optical properties of B are not likely to be because of polaronic (charge-separated ground state) or similar *intramolecular* effects. We note that it might also be interesting to impose certain non-optimized geometries, in order to check for any possibilities of ground-state charge separation, although this is considered to be beyond the scope of the present paper.
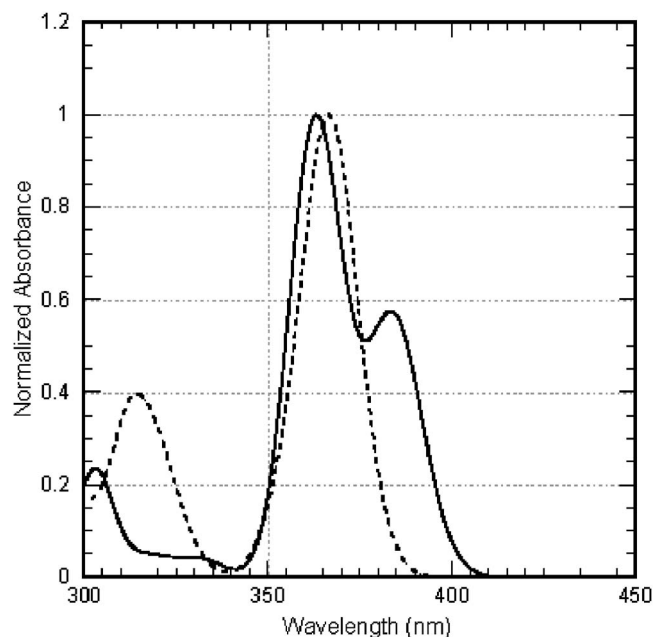
FIG. 7. Absorption spectra of compounds A (solid line) and B (dashed line) calculated at the INDO/SCI level, in which the absorption features are homogeneously broadened by Gaussian functions with a full width at half maximum of 0.15 eV.

However, such ground-state charge transfer seems unlikely as the redox potentials do not indicate that this would be a stable state.

V. DEVICE CHARACTERIZATION

In order to investigate the basic carrier transport properties of the materials under study, TFT studies were carried out to determine the key parameters of carrier type and mobility. The substrates consisted of a ~300 nm thick buffer layer of silica on top of heavily doped silicon, acting as the gate contact layer (Fig. 8, inset). Transistor electrode patterns (30 nm thermally evaporated Au) were prepared on the substrate using standard photolithography techniques. Channel lengths (L) of between 2 and 20 μm were reproducibly possible and the device was designed with inter-digitated electrodes, giving long device widths (W) of 10 000 μm and device capacitances of ~11 nF/cm^2. The prepared substrates were finally treated with O_2 plasma, thus removing any residual adsorbates, then with hexamethyldisilizane (HMDS) in order to promote the necessary hydrophobic wetting. Thin films of the pentaphenylene materials under scrutiny were spin coated on top of the substrates from xylene solution (~ few mg/ml), giving films of thickness 50–60 nm.

Figure 8 shows TFT data for materials A and B and the reference material C, showing A to exhibit p-type behavior in transfer, with an inferred linear regime mobility of 2 $\times 10^{-5}$ cm^2/V s and a threshold gate voltage of −10 V. C also showed p-type behavior with mobility of approximately 1×10^{-5} cm^2/V s and an adversely very high threshold voltage of around −60 V. The behavior of material B is radically different, with the lack of any transconductance indicating insulatorlike properties. We note that such insulating behavior is typical in systems of donor-acceptor complexes,[28] and
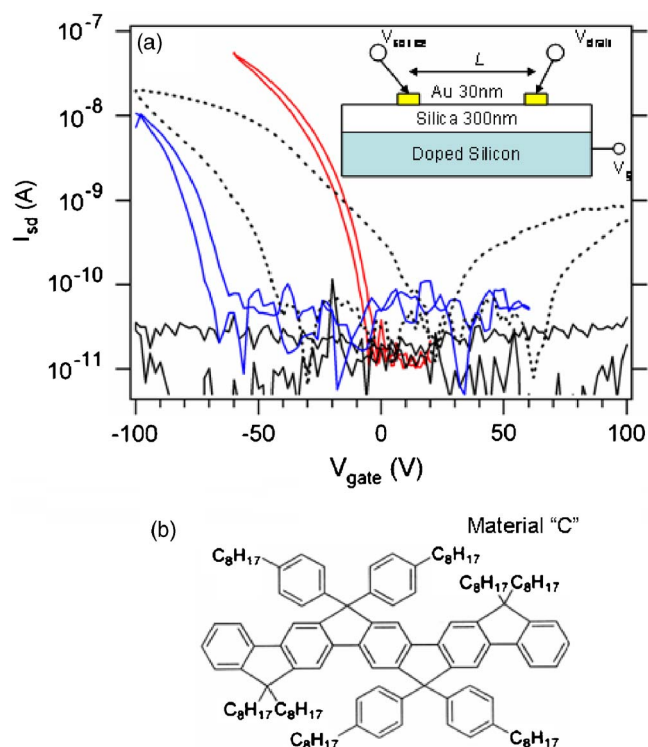

FIG. 8. (Color online) (a) Thin-film transistor (TFT) transfer characteristics for materials A (red line), B (black line) and the pentaphenylene reference material C (blue line). All measurements were made on devices of channel length 2 μm and channel width 10 000 μm, and with a source-drain bias of 40 V. The inferred hole carrier mobilities of materials A and C are of order 10^{-5} cm^2/V s, whereas material B shows the properties expected of an insulator. Also shown is a similar transfer plot, with source-drain bias of 20 V, for a material A device, where the Au electrodes had been pretreated with a thiol-based self-assembled monolayer (dashed line). There is evidence of some electron transconductance, in addition to hole transport. The inset shows a schematic of the bottom-gate transistor design used for these experiments. (b) The chemical structure of material C is shown for reference.

these observations correlate with our initial optical and photophysical measurements. Hence, we consider that the charge-carrier transport properties in these materials are very dependent on the nature of the connectivity of these units to the main pentaphenylene chain, with material A being a favorable design, with respect to both the material B design and the pentaphenylene reference material C.

As a further series of experiments, and in recognition of the large injection barrier which we expect to exist between the Au electrodes (work function in the range of 4.7–5.1 eV) and the semiconducting materials being studied, the TFT substrates were treated with a solution of 1-decanethiol in isopropanol after the HMDS treatment step. This was done in order to deposit a self-assembled monolayer (SAM), as the thiol functional groups will bind strongly to noble-metal surfaces. Previous studies have shown such SAMs to raise the effective work function of Au electrodes by up to 1.0 eV.[29] In Fig. 8, the modified device characteristics for material A are presented, now showing evidence of ambipolarity, with a low mobility electron (n-type) transconductance as well as the p-type transport previously seen. The device characteristics also exhibited an increased hysteresis between the upward and downward measurement scans and we believe this
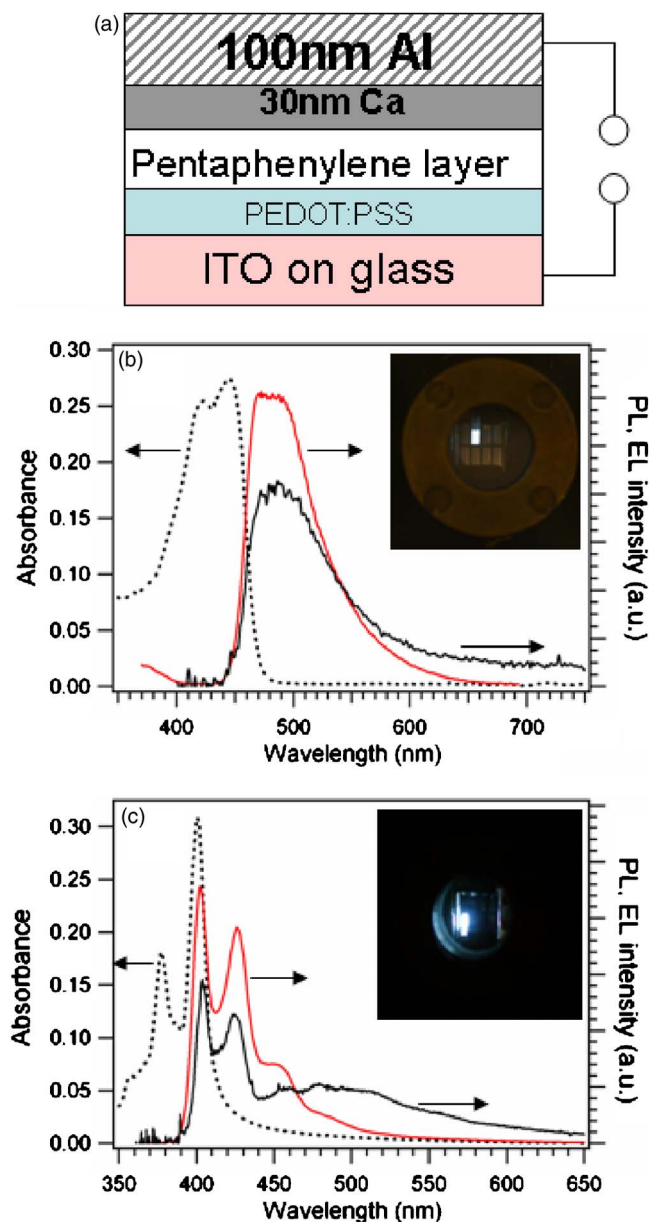
FIG. 9. (Color online) (a) Schematic of the LED structures used for electroluminescence characterization. (b) Measured EL (solid black line) and PL (red line) for material A, together with the thin-film absorption spectrum for reference (dotted black line). The inset shows a digital photograph of an operating device under conditions of normal room light (inset). An excitation wavelength of 350 nm was used in the PL measurements. (c) Thin-film absorption (dotted black line), EL (solid black line), and PL (red line) for the pentaphenylene reference material C, together with a digital photograph of an operating device in a darkened laboratory (inset).

to be due to changes in the wetting properties of the substrate and, commensurately, an increase in the interfacial trapping of charges.

Our light-emitting diodes for EL characterization consisted of a basic planar structure, as shown in Fig. 9(a). A thin layer of poly(3,4-ethylenedioxythiophene)/poly (styrenesulfonate) (PEDOT:PSS) was spin coated onto ITO-coated glass, as the hole-injecting semitransparent electrode. Thin films of the pentaphenylene materials were then spin coated from xylene solution onto the PEDOT:PSS layer. The electron-injecting electrode was then added by thermally evaporating 30 nm of a low work function metal, such as Ca,

and a final protective layer of 100 nm Al was also added by thermal evaporation. The prepared LED devices were not encapsulated, but were carefully stored in a dry nitrogen glovebox and tested under vacuum conditions at room temperature. The device testing was performed using a high-sensitivity parameter analyzer and a spectrally calibrated photodiode. EL spectra were recorded using a fiber-coupled charge coupled device spectrometer, with a spectral resolution of a few nanometers. By way of comparison, PL spectra were measured from control films of the material, which had been spin coated onto standard quartz optical substrates.

The EL emission from material A devices is subjectively blue/green in color, with *Commission Internationale de l'Eclairage* (CIE) chromaticity coordinates $x=0.181$ and $y=0.384$, as calculated from the EL spectrum in Fig. 9(b), and is also found to closely resemble the corresponding PL spectrum. The EL emission from material C devices is subjectively blue/indigo in color, with CIE coordinates $x=0.188$ and $y=0.224$, as calculated from the EL spectrum in Fig. 9(c), and also exhibits the same spectral peaks as in PL, but with a notable longer wavelength component between $\lambda=450$ and 600 nm. We believe that this extra feature may be due to the effects of intermolecular π-π stacking in this case.[30] The EL spectra were also essentially independent of the driving voltage, above the diode switch-on threshold. As was expected, following the preparatory TFT characterization, the use of material B as the active layer did not produce working LED devices.

While the PL efficiencies (or quantum yields) of these all-in-one materials are found to be in the range of 80%–90% in solution and a few percent in thin films, the EL efficiencies of our basic devices are not found to be in a range comparable with the best reported organic LEDs (OLEDs).[31,32] Using appropriate calibration parameters to account for the spectral response function of the photodiode detector and the standard eye response function, we typically see surface brightness of order $10-100$ cd/m^2 at relatively high driving voltages of $5-10$ V, current efficiencies of order $0.01-0.1$ cd/A, and external quantum efficiencies of up to 0.1%. A major constraint on the device performance is the very thin nature of the films which may be spin coated from solutions of such oligomeric materials, which have a much lower viscosity than solutions of conjugated polymers, for example. Profilometry studies indicate the active layers to be of thickness of order 30 nm only, with a significant roughness. This is likely to result in the device performance being affected by "pin holes" and the generation of very large electric fields across the active layer, giving a reduced current-to-light performance and explaining the gradual degradation of devices over the course of prolonged operation. More sophisticated LED designs, such as the use of carrier blocking layers[33,34] and suitable matrix media might allow the device performance to be significantly optimized, taking full advantage of the favorable electrochemical and light-emitting properties of these all-in-one materials.

VI. SUMMARY AND CONCLUSIONS

Two new ladder-type pentaphenylenes, bearing both electron-donating triphenylamine and electron-accepting

oxadiazole substituents, have been prepared. We have reported upon optical and photophysical studies of these systems and demonstrated that donor-acceptor interactions are very dependent on the nature of the connectivity of these groups to the main pentaphenylene chain. Of particular interest, we observe luminescent emission with a biexponential decay and unusually long lifetimes of order 10 ns, which are characteristic of exciplex-like states of these molecules.

One such structure, in which the oxadiazole groups were attached as side chains and the amines at the ends of the molecule, shows absorption which is redshifted from that of the pentaphenylene due to delocalization onto the end groups, and highly efficient PL. By contrast, the other structure, where the electron-donating and -accepting substituents were directly opposite each other as side chains on the molecule, shows strong absorption in a band around 700 nm and comparatively low PL efficiency. Quantum-chemical modeling confirms that this different behavior must arise from intermolecular donor-acceptor interactions, rather than intramolecular charge separation. Chemical and electrochemical tests suggest an intermolecular aggregation, which is mediated by oxidative processes, in dynamic equilibrium with the monomer.

We consider that such materials might serve both as model compounds for new polymers or as emissive materials in their own right. Further elaborate tailoring of intra- and interchain interactions, including push-and-pull mechanisms, between the conjugated backbone and substituents is anticipated. Such optimized designs may also allow such materials to be prototypical analog structures for considering more complex *multichromophoric* systems (e.g., polyisocyanopeptides[35]) for "light-harvesting" applications,[36] for example.

The observation of a robust blue or blue/green electroluminescence in simple, nonoptimized LED configurations suggests that these materials represent a new and interesting category of oligomeric semiconductors for future application in LEDs. OLEDs are one of the most important emerging optoelectronics technologies[37,38] and we believe that these materials present new opportunities for ways in which the photophysics and charge-accepting abilities of the light-emitting media may be optimized in order to improve the efficiency of devices.

APPENDIX: SYNTHESIS OF PENTAPHENYLENE STRUCTURES

1. Addition of oxadiazole to pentaphenylene diester 1

A solution of 2-(4′-tert-butylphenyl)-5-(4′-bromophenyl-1,3,4-oxadiazole (3.66 g, 10.2 mmol) in dry tetrahydropuran (THF) (50 mL), in a 250 mL Schlenk flask, was cooled to −78 °C. N-butyllithium in hexane (9.26 mL,

14.8 mmol, 1.6M in hexane) was then added and the mixture was stirred for 20 min. Then a solution of the compound 1 (2 g, 2.05 mmol) in dry THF (40 mL) was added dropwise with stirring, and the solution was slowly allowed to warm to room temperature. The mixture was extracted with diethyl ether, and the extract was washed with brine and dried over MgSO$_4$. The crude product was purified by column chromatography on silica gel with hexane and ethyl acetate (v/v:2:1) as eluent to give the diol 3 as a light yellow solid (1.75 g, 42%). FDMS (Field Desorption Mass Spectroscopy): m/z 2023.5 $[M^+]$ (calculated: 2020.75). Further elution with hexane and ethyl acetate (v/v:7:1) gave the diadduct 4 as a light yellow solid (1.00 g, 33%). FDMS: m/z 1497.4 $[M^+]$ (calculated: 1496.09)

2. Synthesis of dioxadiazole attached pentaphenylene 5

The diadduct 4 (1.3 g, 0.86 mmol) was dissolved in dichloromethane (30 mL), and BF$_3$ etherate (0.05 mL) was added with stirring at room temperature. The mixture solution was then refluxed overnight. The solution was concentrated and poured dropwise into methanol; the product started to precipitate as a white solid. The mixture was stirred for 12 h and the solid was collected by filtration, washed with methanol, and dried. The product was redissolved in dichloromethane and precipitated again from methanol. Yield: 1 g (78%). FDMS: m/z 1477.8 $[M^+]$ (calculated: 1478.08).

3. Synthesis of dioxadiazole and di-triphenylamine attached phentaphenylene 7

A solution of 4-bis(4′-octylphenyl) amino-1-bromobenzene (0.82 g, 1.5 mmol) in dry THF (30 mL), in a 250 mL Schlenk flask, was cooled to −78 °C. N-butyllithium in hexane (1.12 mL, 1.8 mmol, 1.6M in hexane) was then added and the mixture was stirred for 20 min. Then a solution of 5 (0.74 g, 0.5 mmol) in dry THF (10 mL) was added dropwise, and the mixture solution was stirred overnight. FDMS analysis of the reaction showed formation of the desired monoalcohol at m/z 2384.6 together with small amounts of ring closed products. Hence, the crude product after workup was used as such in the next step. This crude product was dissolved in dichloromethane (20 mL), and several drops of BF$_3$ etherate was added with stirring at room temperature. The solution turned deep green immediately upon addition and the reaction was quenched with methanol. The product was precipitated as a deep green solid. The solid was purified by column chromatography on silica gel with methylene chloride and ethyl acetate (v/v:1:1) as eluent to give the compound 7 as a deep green solid (0.25 g, 21% for two steps). FDMS: m/z 2368.7 $[M^+]$ (calculated: 2367.51).

4. Synthesis of tetraoxadiazole attached pentaphenylene 8

The diol 3 (1 g, 0.5 mmol) was dissolved in dichloromethane (10 mL), and BF$_3$ etherate (0.05 mL) was added with stirring at room temperature. The colorless solution

turned brown immediately upon addition and became light yellow within minutes. After 10 min, the solution was concentrated and dropwise into methanol. The product started to precipitate as a solid. The mixture was stirred for 12 h and the solid was collected by filtration, washed with methanol, and dried. The product was redissolved in dichloromethane and reprecipitated from methanol to give the pentaphenylene **8**. Yield: 0.87 g (89%). FDMS: m/z 1986.7 $[M^+]$ (calculated: 1984.72).

5. Synthesis of dibromopentaphenylene 9

The pentaphenylene **8** (1.2 g, 0.6 mmol) was dissolved in 50 mL of dichloromethane and cooled in an ice bath. Then bromine (0.58 g, 3.62 mmol) was added and the solution was stirred overnight at room temperature with monitoring by FDMS analysis. The reaction mixture was cooled and the resulting white precipitate was collected, and recrystallized from chloroform and ethyl acetate, to give the dibromide **9** as a white powder (0.98 g, 76%). FDMS: m/z 2143.8 $[M^+]$ (calculated: 2142.51).

6. Synthesis of tetraoxadiazole pentaphenylene 10

The pentaphenylene **9** (0.4 g, 0.18 mmol), di(4-methoxyphenyl)amine (98 mg, 0.42 mmol), and sodium *tert*-butoxide (43 mg) were mixed in a flask. The flask was evacuated, refilled with argon, and then $Pd(OAc)_2$ (22 mg), $PtBu_3$ (75 mg), and dry toluene (30 mL) were added. The mixture was heated to 100 °C with stirring overnight. The reaction mixture was then cooled to room temperature, diluted with H_2O, and extracted with toluene. The combined organic fractions were washed with brine and then dried over $MgSO_4$. Removal of solvent afforded the crude product, which was further purified by column chromatography on silica gel with methylene chloride and ethyl acetate (v/v:9:1) to give compound **10** as a yellow solid (0.28 g, 62%). FDMS: m/z 2439.9 $[M^+]$ (calculated: 2439.24).

7. NMR analysis

a. Structure 7

1H NMR (CDCl3, 400 MHz) $\delta = 8.09$ (*d*, 8H), 8.01 (*d*, 8H), 7.81 (*s*, 4H), 7.66 (*s*, 2H), 7.65 (*m*, 4H), 7.51 (*d*, 4H), 7.49 (*d*, 4H), 7.35 (*d*, 2H), 7.30 (*d*, 2H), 7.18 (*d*, 4H), 7.10 (*d*, 4H), 7.1–6.8 (*m*, 8H), 2.55 (*t*, 8H), 1.55 (*m*, 8H), 1.29 (*m*, 18H), 1.20–0.90 (*m*, 96H), 0.9–0.55 (*m*, 24H).

b. Structure 10

^{1}H NMR (CDCl3, 400 MHz) $\delta = 8.10$ (*d*, 8H), 8.00 (*d*, 8H), 7.81 (*s*, 4H), 7.65 (*s*, 2H), 7.57 (*d*, 8H), 7.51 (*d*, 8H), 7.41 (*s*, 2H), 7.16–6.50 (*m*, 20H), 3.78 (*s*, 12H), 1.88 (*m*, 8H), 1.35 (*s*, 36H) 1.20–0.96 (*m*, 40H), 0.76 (*t*, 12H), 0.73–0.64 (*m*, 8H).

[1] J. Jacob, S. Sax, T. Piok, E. J. W. List, A. C. Grimsdale, and K. Müllen, J. Am. Chem. Soc. **126**, 6987 (2004).

[2] J. Jacob, S. Sax, M. Gaal, E. J. W. List, A. C. Grimsdale, and K. Müllen, Macromolecules **38**, 9933 (2005).

[3] Z. He, W. Y. Wong, X. Yu, H. S. Kwok, and Z. Lin, Inorg. Chem. **45**, 10922 (2006).

[4] C. H. Chien, P. I. Shih, F. I. Wu, C. F. Shu, and Y. Chi, J. Polym. Sci., Part A: Polym. Chem. **45**, 2073 (2207).

[5] A. C. Morteani, R. H. Friend, and C. Silva, Chem. Phys. Lett. **391**, 81 (2004).

[6] A. C. Morteani, P. Sreearunothai, L. M. Herz, R. H. Friend, and C. Silva, Phys. Rev. Lett. **92**, 247402 (2004).

[7] C. Ego, A. C. Grimsdale, F. Uckert, G. Yu, G. Srdanov, and K. Müllen, Adv. Mater. (Weinheim, Ger.) **14**, 809 (2002).

[8] T. Miteva, A. Meisel, W. Knoll, H. G. Nothofer, U. Scherf, D. C. Müller, K. Meerholz, A. Yasuda, and D. Neher, Adv. Mater. (Weinheim, Ger.) **13**, 565 (2001).

[9] F.-I. Wu, S. Reddy, C.-F. Shu, M. S. Liu, and A. K.-Y. Jen, Chem. Mater. **15**, 269 (2003).

[10] C.-F. Shu, R. Dodda, F.-I. Wu, M. S. Liu, and A. K.-Y. Jen, Macromolecules **36**, 6698 (2003).

[11] A. C. Grimsdale and K. Müllen, Angew. Chem., Int. Ed. **44**, 5592 (2005).

[12] Y. Fang, S. Gao, X. Yang, Z. Shuai, D. Beljonne, and J. L. Bredas, Synth. Met. **141**, 43 (2004).

[13] P. J. Skabara, R. Berridge, I. M. Serebryakov, A. L. Kanibolotsky, L. Kanibolotskaya, S. Gordeyev, I. F. Perepichka, N. S. Sacrifitci, and C. Winder, J. Mater. Chem. **17**, 1005 (2007).

[14] K. Feng, L.-Z. Wu, L.-P. Zhang, and C.-H. Tung, Dalton Trans. 2007, 3991.

[15] J. R. Lakowicz, *Principles of Fluorescence Spectroscopy* (Kluwer Academic/Plenum, New York, 1999).

[16] W. Becker, *Advanced Time-Correlated Single Photon Counting* (Springer-Verlag, Berlin, 2005).

[17] H. J. Snaith, G. L. Whiting, B. Sun, N. C. Greenham, W. T. S. Huck, and R. H. Friend, Nano Lett. **5**, 1653 (2005).

[18] A. C. Morteani, Ph.D. thesis, University of Cambridge, 2004.

[19] S. Janietz, D. D. C. Bradley, M. Grell, C. Giebeler, M. Inbasekaran, and E. P. Woo, Appl. Phys. Lett. **73**, 2453 (1998).

[20] W. L. Yu, J. Pei, Y. Cao, W. Huang, and A. J. Heeger, Chem. Commun. (London) **18**, 1837 (1999).

[21] C. Tang, F. Liu, Y. J. Xia, L. H. Xie, A. Wei, S. B. Li, Q. L. Fan, and W. Huang, J. Mater. Chem. **16**, 4074 (2006).

[22] M. J. S. Dewar, E. G. Zoebisch, E. F. Healy, and J. J. P. Stewart, J. Am. Chem. Soc. **107**, 3902 (1985).

[23] M. C. Zerner, G. H. Loew, R. Kichner, and U. T. Mueller-Westerhoff, J. Am. Chem. Soc. **102**, 589 (1980).

[24] M. C. Zerner, G. H. Loew, R. Kichner, and U. T. Mueller-Westerhoff, J. Am. Chem. Soc. **122**, 3015 (2000).

[25] J. Cornil, I. Gueli, A. Dkhissi, J. C. Sancho-Garcia, E. Hennebicq, J. P. Calbert, V. Lemaur, D. Beljonne, and J. L. Bredas, J. Chem. Phys. **118**, 6615 (2003).

[26] K. G. Jesperson, W. J. D. Beenken, A. Zaushitsyn, A. Yartsev, M. Andersson, T. Pulleritis, and V. Sundstrom, J. Chem. Phys. **121**, 12613 (2004).

[27] J. Sancho-Garcia, C. L. Foden, I. Grizzi, G. Greczynski, M. P. deJong, W. Salaneck, J. L. Bredas, and J. Cornil, J. Phys. Chem. B **108**, 5594 (2004).

[28] T. Ishiguro, K. Yamaji, and G. Saito, *Organic Semiconductors*, 2nd ed. (Springer-Verlag, Berlin, 1998).

[29] I. H. Campbell, S. Rubin, T. A. Zawodzinski, J. D. Kress, R. L. Martin, D. L. Smith, N. N. Barashkov, and J. P. Ferraris, Phys. Rev. B **54**, R14321 (1996).

[30] X. Chen, H. E. Tseng, J. L. Liao, and S. A. Chen, J. Phys. Chem. B **109**, 17496 (2005).

[31] Y. Zhang, F. He, G. Cheng, C. Ruan, Y. Lin, Y. Zhao, Y. Ma, and S. Liu, Semicond. Sci. Technol. **22**, 214 (2007).

[32] H. Yersin, *Highly Efficient OLEDs with Phosphorescent Materials* (Wiley-VCH, Weinheim, 2007).

[33] G. Yu, X. Xu, Y. Liu, Z. Jiang, S. Yin, Z. Shuai, D. Zhu, X. Duan, and P. Lu, Appl. Phys. Lett. **87**, 222115 (2005).

[34] Y. J. Su, H. L. Huang, C. L. Li, C. H. Chien, Y. T. Tao, P. T. Chou, S. Datta, and R. S. Liu, Adv. Mater. (Weinheim, Ger.) **15**, 884 (2003).

[35] J. Hernando, P. A. J. de Witte, E. M. H. P van Dijk, J. Korterik, R. J. M. Nolte, A. E. Rowan, M. F. Garcia-Parajó, and N. F. van Hulst, Angew. Chem., Int. Ed. **43**, 4045 (2004).

[36] M. F. García-Parajó, J. Hernando, G. S. Mosteiro, J. P. Hoogenboom, E. M. H. P. van Dijk, and N. F. van Hulst, ChemPhysChem **6**, 819 (2005).

[37] A. Kraft, A. C. Grimsdale, and A. B. Holmes, Angew. Chem., Int. Ed. **37**, 402 (1998).

[38] U. Mitschke and P. J. Bäuerle, J. Mater. Chem. **10**, 1471 (2000).